

# Gel-Type Polyacrylic Resins Cross-Linked with Trimethylolpropane-trimethacrylate: The Issue of Their Nanostructure and Molecular Accessibility Unveiled with a Combination of Inverse Steric Exclusion Chromatography (ISEC), and ESR and CP-MAS $^{13}\text{C}$ NMR Spectroscopy

Franco Pozzar,<sup>[a]</sup> Alessandro Sassi,<sup>[b]</sup> Giuseppe Pace,<sup>[b]</sup> Silvano Lora,<sup>[c]</sup> Angelo Antonio D'Archivio,<sup>\*,[d]</sup> Karel Jeřábek,<sup>[e]</sup> Alfonso Grassi,<sup>\*,[f]</sup> and Benedetto Corain<sup>\*,[a]</sup>

**Abstract:** Six gel-type functional resins, that is, three poly-DMAA-*co*-TMPTP (DMAA = *N,N*-dimethylacrylamide, TMPTP = trimethylolpropyltrimethacrylate) samples with different degrees of cross-linking (0.6, 1.2, 1.7% mol) and three poly-DMAA-*co*-MA-*co*-TMPTP (MA = methacrylic acid, ca. 5.5% mol) samples with 1.7, 3.5, and 7% mol cross-linking were investigated with ISEC (inverse steric exclusion

chromatography), and ESR and CP-MAS (cross polarization magic angle spinning)  $^{13}\text{C}$  NMR spectroscopy after swelling in water and other solvents. This unprecedented combination of

conceptually independent physico-chemical techniques provides a thorough overall consistent picture of the morphology of the resins on the nanometer scale and of the molecular accessibility of the swollen polymer framework to the paramagnetic probe TEM-PONE (2,2,6,6-tetramethyl-4-oxo-1-oxypiperidine) and to selected solvents.

**Keywords:** EPR spectroscopy • functional resins • ISEC (inverse steric exclusion chromatography) • nanostructures • NMR spectroscopy

## Introduction

The most commonly employed supported metal catalysts that are active in the liquid phase are materials built up with an inorganic support or active carbon, and a nanoclustered metal(0) component. In some cases the support may exert

also a co-catalytic effect.<sup>[1]</sup> In the early seventies, organic supports such as functional resins,<sup>[2–4]</sup> started to be considered as valid alternatives to inorganic ones, and M<sup>0</sup>/resin nanocomposites have been successfully tested in reactions relevant to fine chemistry and specialty chemicals applications and, at least in one case, they are currently used for

[a] Dr. F. Pozzar, Prof. B. Corain  
Dipartimento di Scienze Chimiche  
Università di Padova  
Via Marzolo 1, 35131 Padova (Italy)  
Fax: (+39)049-8275223  
E-mail: benedetto.corain@unipd.it


[b] Dr. A. Sassi, Dr. G. Pace  
Istituto di Scienze e Tecnologie Molecolari, C. N. R.  
Sezione di Padova, Via Marzolo 9, 35131 Padova (Italy)

[c] Dr. S. Lora  
ISOF, Istituto per la Sintesi Organica e la Fotoreattività  
CNR, Sezione di Legnaro, Viale dell'Università 1  
35020 Legnaro, Padova (Italy)

[d] Prof. A. A. D'Archivio  
Dipartimento di Chimica Ingegneria Chimica e Materiali  
Università di L'Aquila, Via Vetoio Coppito Due  
67010 L'Aquila (Italy)  
Fax: (+39)0862-43-3753  
E-mail: darchivi@ing.univaq.it

[e] Dr. K. Jeřábek  
Institute of Chemical Process Fundamentals  
Czech Academy of Sciences  
165 02 Suchbát-Praha 6 (Czech Republic)

[f] Prof. A. Grassi  
Dipartimento di Chimica  
Università di Salerno Via S. Allende  
84081 Baronissi (Italy)  
Fax: (+39)089-965296  
E-mail: agrassi@unisa.it

 Supporting information for this article is available on the WWW under <http://www.chemeurj.org/> or from the author.

the industrial synthesis of a semicommodity (i.e., methylisobutylketone).<sup>[5]</sup> In these innovative metal catalysts, metal nanoclusters are designed to be dispersed inside a designable polymer framework (Figure 1). The support is thus ex-

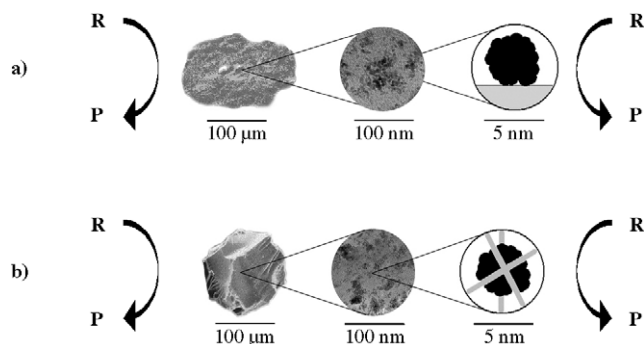


Figure 1. Schematic comparison between a conventional nanostructured metal catalyst supported on a conventional inorganic framework (a) or inside a functional resin organic framework (b).

pected to play a role in controlling the access of the reagents (R) to the metal surface, the transport of the products (P) to the bulk liquid phase (Figure 1) and even to exert a possible effect on the thermodynamics and the kinetics of the reaction itself.<sup>[6]</sup>

In addition to the results published in the past decade and reviewed by Corain and Kralik in 2000<sup>[5]</sup> (among which we mention a very elegant paper appeared in 1991 by Toshima and associates<sup>[7]</sup>) and from those stemming from our own recent experience,<sup>[8–10]</sup> we would like to mention the recent contributions by Shi and Deng,<sup>[11]</sup> and by Uozumi and Nakao.<sup>[12]</sup> In addition to these last promising results, Fierro and associates have recently reported<sup>[13]</sup> on the successful direct synthesis of hydrogen peroxide from dihydrogen and dioxygen in methanol/water mixtures in the presence of pal-

ladium/resin (resin=Lewatit K 2641 in acidic form) catalysts. While the authors stipulate that the metal is present as a “Pd<sup>2+</sup>” species, specific tests carried out in these laboratories strongly suggest that the remarkable activity of Fierro’s catalysts is due to the presence of nanoclustered Pd<sup>0</sup> already present in the as-prepared catalyst.<sup>[14]</sup>

Cross-linked polymer materials utilised so far as supports of metal nanoclusters are normally classified as gel- or macroreticular-type.<sup>[4]</sup> However, regardless of their micro- and nanomorphology differences, in both cases the individual metal nanoclusters eventually experience comparable problems of accessibility on the nanometer scale (Figure 2).

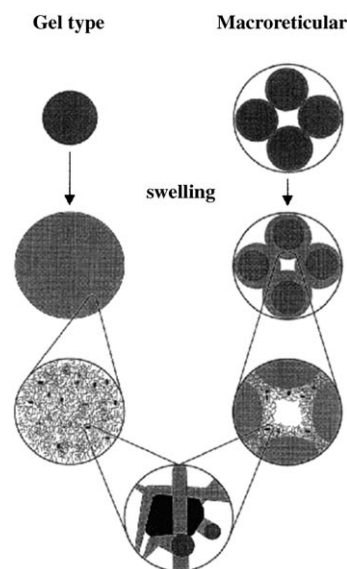


Figure 2. Schematic pictures of nanometer level morphology of gel-type and of macroreticular resins in the swollen state. Metal nanoclusters are indicated as black spots.

It seems reasonable to state that the most useful design and the best utilization of this type of supported metal catalyst rests on a thorough knowledge of 1) the structure of the relevant supports in their working state (i.e., in their swollen state) on the nanometer scale and 2) their molecular accessibility to solvent molecules and to reagents of substantial size. In this context, we have been active for more than one decade in the synthesis of properly designed gel-type resins built up with acrylic comonomers cross-linked with bifunctional cross-linking agents, typically *N,N*-methylenebisacrylamide.<sup>[8]</sup> We have developed our program so far upon taking advantage of  $\gamma$ -rays-induced polymerization,<sup>[4]</sup> and we have established a multimethodological approach to the quantitative evaluation of the nanostructure and molecular accessibility of our materials after swelling in suitable solvents. Our so far established tools are inverse steric exclusion chromatography (ISEC),<sup>[15]</sup> ESR spectroscopy of stable radical penetrating the nanoporous domains of the swollen materials<sup>[16–17]</sup> and pulse field-gradient spin-echo (PGSE) NMR analysis of the resins after full swelling in given solvents.<sup>[18–19]</sup> ESR and PGSE NMR spectroscopy provide de-

**Abstract in Italian:** Sei resine funzionali di tipo gel del tipo poli-DMAA-co-TMPTP (DMAA = *N,N*-dimetilacrilammide, TMPTP = trimetilolpropiltrimetacrilato) caratterizzate da diversi gradi di reticolazione (0.6, 1.2, 1.7% mol) e del tipo poli-DMAA-co-MA-co-TMPTP (MA = acido metacrilico ca 5.5 - % mol) con grado di reticolazione 1.7, 3.5, 7% sono state studiate tramite ISEC (inverse steric exclusion chromatography), ESR e CP-MAS (cross polarization magic angle spinning) <sup>13</sup>C NMR dopo rigonfiamento in acqua e altri solventi. Questa inedita combinazione di tecniche chimico-fisiche, concettualmente indipendenti tra loro, offre una descrizione complessiva e consistente della loro morfologia nanometrica e una valutazione quantitativa dell'accessibilità dei loro reticoli polimerici sia alla sonda paramagnetica TEM-PONE sia alle molecole di opportuni solventi.

tailed information on the rotational mobility of given paramagnetic probes and on the translational mobility of given molecules in the interior of nanoporous materials, respectively. ISEC is an extremely useful tool to assess the nanometer scale morphology of swollen polymer frameworks in terms of either the model designed by Ogston, based on the space occupancy by the solvated polymer chains (polymer chain concentration,  $\text{mm}^{-3}$ ),<sup>[20]</sup> or of the conventional cylindrical pore model<sup>[15d]</sup> (see later for details). The relevance of these conceptual and physical tools to metal catalysis technology has been recently highlighted by us.<sup>[21–24]</sup> Inter alia, we have in fact discovered that functional resins, thanks to their controllable nanoporosity, can behave as templates in the production of size-controlled metal nanoclusters (template controlled synthesis approach);<sup>[22]</sup> this fact is relevant for applications in chemical processing.

We report in this paper on the synthesis of acrylic resins composed of the trifunctional cross-linking agent trimethylolpropanetrimesic acid (TMPTMA), the structural comonomer *N,N*-dimethylacrylamide (DMAA) and the functional comonomer methacrylic acid (MA). The specific aims of this paper are 1) a verification of our multimethodological approach to provide convergent and quantitative information on the nanostructure of swollen gel-type resins, 2) the critical and comparative inclusion of another powerful analytical tool, that is, CP-MAS <sup>13</sup>C NMR and 3) the evaluation of the effect of a trifunctional cross-linker on the overall morphology of the resins in their swollen state. It should be pointed out that TMPTMA has been already employed as cross-linker to produce macroreticular resins based on glycidyl methacrylate,<sup>[25–27]</sup> one of which resin was characterised with ISEC.<sup>[25]</sup>

## Results and Discussion

Figure 3 illustrates the structure and Table 1 gives the molar composition and labelling nomenclature (MASF and AAD) of the investigated resins. For details about synthesis and polymerisation yields, see the Experimental Section.

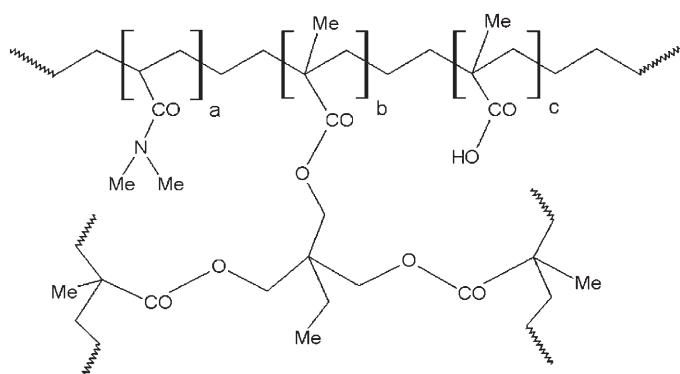


Figure 3. Schematic representation of the structure of resins AAD and MASF. Theoretical molar fractions of DMAA (a), TMPTMA (b) and MA (c) are given in Table 1.

Table 1. Molar composition [%] of synthesised resins.<sup>[a]</sup>

	DMAA	TMPTMA	MA
MASF2	99.4	0.6	0.0
MASF4	98.8	1.2	0.0
MASF6	98.3	1.7	0.0
AAD1	93.1	1.7	5.2 (0.53 meq g <sup>-1</sup> )
AAD2	91.1	3.5	5.4 (0.51 meq g <sup>-1</sup> )
AAD3	87.2	7.0	5.8 (0.50 meq g <sup>-1</sup> )

[a] For the structures of DMAA, TMPTMA, and MA in the polymer see Figure 3.

Resins in the form of colourless particles (400–180  $\mu\text{m}$ ) were examined as such, apart from the case of ISEC measurements that require a smaller size (<180  $\mu\text{m}$ ). Polymerisation yields were near to 95% as expected from previous experience<sup>[8]</sup> and elemental analyses were consistent with the composition of the reaction mixtures, again in line with the known close similarity of the reactivities of the involved comonomers.

**Thermal behaviour (TGA):** All resins were investigated under identical conditions (see Experimental Section), and for MASF6 and AAD1 TGA analysis was coupled with IR monitoring of the gaseous products stemming from the heated samples. The MASF resins exhibit a somewhat greater thermal stability than resins AAD (Figure 4). The thermal stability of the AAD resins appears to increase appreciably with the increase in the degree of cross-linking.

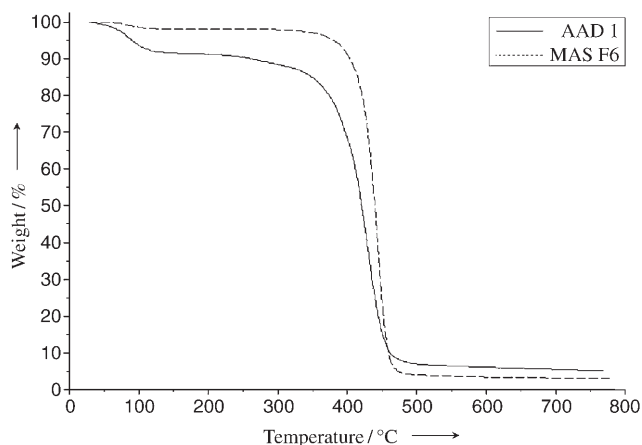


Figure 4. TGA profile of resin AAD1 and MASF6; 20 °C min<sup>-1</sup> under nitrogen.

For the AAD series in the gas phase, the IR spectra reveal that resin decomposition is in fact a thermal depolymerization (Figures 5 and 6, see also the Supporting Information).

For all investigated resins, the presence of a significant amount of carbon dioxide (the relative abundance of which increases with the temperature) is interpreted as the consequence of the concomitant thermal decomposition of the cross-linker.

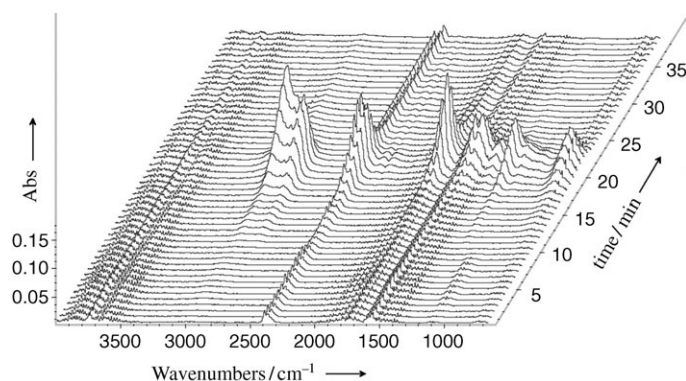


Figure 5. Gas evolution during TGA runs from AAD1. IR spectra are recorded from 40 °C to 800 °C at 20 °C min<sup>-1</sup> under nitrogen at a sampling frequency equal to one spectrum every 30 s, with a spectral resolution of 4 cm<sup>-1</sup>.

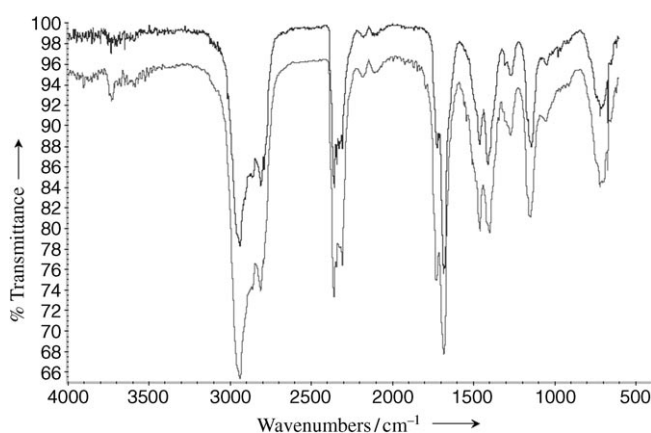


Figure 6. FTIR of gases released at approximately 430 °C during TGA runs from: AAD1 (lower spectrum) and from homopolymerised *N,N*-dimethylacrylamide generated in the thermobalance during the TGA-DTA of the monomer (upper spectrum). See also the Supporting Information.

#### Nanometer-level morphology in water—ISEC analysis:

ISEC provides detailed information on the swollen-state morphology of cross-linked polymers. It is based on the analysis of elution behaviour of standard solutes with known effective molecular size flowing through a column filled with the investigated material, under conditions in which the chromatographic process is influenced by steric (entropic) effects only. Similarly to the case of the other porosimetric methods, the mathematical treatment of the elution data is based on the depiction of the morphology of the investigated material by using a simple geometrical model. It has been proved that the morphology of swollen polymer gels is best described on the basis of the so-called Ogston's model,<sup>[20]</sup> depicting pores as spaces among randomly oriented rigid rods. This simplified depiction of the morphology of swollen polymer networks provides a fair description of both the intensive parameters (polymer chain densities) and extensive properties (specific volumes of variously dense polymer fractions). On the other hand, the basic character of the much more common cylindrical pore model depicting

pores as cylindrical holes in solid matter differs from the physical reality of the polymer framework geometry rather substantially. However, although the description of the swollen morphology of a polymer matrix based on the cylindrical pore model produces unrealistic values for the pores volumes (extensive properties), it provides a useful description of the porosity in terms of pores diameter distribution (intensive property). The ISEC data are collected in Tables 2 (Ogston's model)<sup>[20]</sup> and 3 (cylindrical pores model).<sup>[19d]</sup>

Table 2. ISEC data for resins MASF and AAD according to Ogston's model.

$c_c$ [mm mm <sup>-3</sup> ] <sup>[a]</sup>	Volume of swollen polymer fractions [cm <sup>3</sup> g <sup>-1</sup> ]				
	MASF4	MASF6	AAD1	AAD2	AAD3
0.1	0.00	0.00	0.00	0.00	0.00
0.2	0.46	0.24	0.22	0.15	0.00
0.4	2.26	0.14	0.51	0.00	0.00
0.8	0.00	0.00	0.00	0.93	0.00
1.5	0.00	2.60	2.16	0.55	0.99
$\Sigma V_i$ [cm <sup>3</sup> g <sup>-1</sup> ] <sup>[b]</sup>	2.73	2.98	2.89	1.63	0.99
$V_{\text{tot,gel}}$ [cm <sup>3</sup> g <sup>-1</sup> ] <sup>[c]</sup>	2.94	2.54	2.55	1.87	1.37

[a] Polymer chain concentration. [b] Total swollen polymer volume calculated as the sum of individual ISEC-detected polymer fractions. [c] Total swollen polymer volume evaluated from column balance (see text for details).

Table 3. ISEC data for resins MASF and AAD according to the cylindrical pores model.

$d$ [nm] <sup>[b]</sup>	Pores volume [cm <sup>3</sup> g <sup>-1</sup> ] <sup>[a]</sup>				
	MASF4	MASF6	AAD1	AAD2	AAD3
0.6	0.37 (0.71)	3.09	2.37	1.32	1.00
1.1	0.00 (0.00)	0.00	0.00	0.00	0.00
1.6	0.00 (0.00)	0.00	0.00	0.00	0.11
2.7	0.00 (0.00)	1.73	1.59	1.00	0.18
3.2	1.61 (1.54)	0.00	0.13	0.11	0.00
4.3	1.22 (0.42)	0.00	0.00	0.00	0.00
8.1	0.02 (0.00)	0.00	0.00	0.00	0.00
19.4	0.00	0.00	0.02	0.00	0.01

[a]  $\Sigma$  of the pore volume [cm<sup>3</sup> g<sup>-1</sup>]: 3.22 MASF4; 2.43 AAD2; 1.30 AAD3. Numbers in parentheses refer to a resin poly-DMAA-MBA (MBA = methylenebisacrylamide, 4.1% mol, reference [23]). [b] Pore diameter.

The comparison between the observed figures for  $V_{\text{tot,gel}}$  and  $\Sigma V_i$  for each resin is a good means to evaluate the overall reliability of ISEC analysis. The parameter  $V_{\text{tot,gel}}$  is the difference between the known volume of the empty ISEC column and the experimentally determined interparticle volume of the resin bed. It is therefore a model-independent, directly determined quantity. The  $\Sigma V_i$  parameter is the sum of volumes of the differently dense fractions (five in this case) that comprise the swollen-state morphology model. Individual  $V_i$  are adjustable parameters of the model, and their values are the result of the mathematical treatment of the elution volumes of standard solutes, aimed

at minimising the differences between the experimentally determined values and those stemming from the model computed. Ideally,  $\Sigma V_i$  should be equal to  $V_{\text{totgel}}$ . If the value of  $\Sigma V_i$  is smaller than that of  $V_{\text{totgel}}$ , a portion of the polymer gel must be so dense that even the smallest of the steric probes ( $D_2O$  in this case) is unable to enter a part of  $V_{\text{totgel}}$ . Consequently, this part of the polymer framework is “invisible” to the chromatography analysis. If, however, the value of  $\Sigma V_i$  is greater than the true polymer gel volume  $V_{\text{totgel}}$ , then the volumes of some of the model parts must be overestimated or the retention of the standard solutes must be influenced not only by entropic (steric) factors, but also by enthalpic (adsorption) interactions. Such discrepancies are usually the result of the presence of the most dense fractions (higher polymer chain concentrations), for which the morphology information is less reliable than for the less dense ones, which are more accessible to the employed steric probes. On the basis of the above discussion, ISEC analysis turns out to be quite reliable for MASF4, AAD2 and AAD3.

The porosity pattern provided by the computation of the observed retention volumes in terms of cylindrical pores, Table 3, is intrinsically less sophisticated (and less physically correct) than that offered by Table 2. However, it turns out to be in fact very useful if ISEC analysis is aimed at predicting the physical ability of the polymer framework to control and limit the size of metal nanoclusters generated inside of it upon spontaneous aggregation of individual metal atoms.<sup>[22]</sup> Thus, although nanopores are not really present in the polymer framework, the framework itself behaves towards the mobility of the steric probes along the column as if cylindrical pores were existing entities.

Keeping this in mind, we note that resins MASF6, AAD1, AAD2 and AAD3 have very narrow pores with an effective diameter of 0.6 nm. Moreover, it is clear that the trend of total volumes of accessible porosity, as quantified by sum of the pore volumes (Table 3) from MASF4 to AAD2 and AAD3 is consistent with the increase of percentage of the degree of cross-linking : (3.22 (1.2%) → 2.43 (3.5%) → 1.30 cm<sup>3</sup>g<sup>-1</sup> (7.0%)). Interestingly, the less cross-linked macromolecular framework (MASF4) also features relatively large pores with effective diameters equal to 3.2 nm (50% of total accessible volume) and to 4.3 nm (38% of total accessible volume). Finally, while 2.7 nm pores are present in MASF6, AAD1, AAD2 and AAD3, their contribution to the overall porosity decreases with the increase of the degree of cross-linking. It can be concluded that both the observed morphological features and the overall trends are essentially consistent with the expectations based on the trend of the molar fractions of TMPTMA involved in the polymerisation process (Table 1). Employment of the trifunctional cross-linking agent does not induce the formation of peculiar morphological features. The swollen state morphology of the resin MASF4 cross-linked with 1.2% mol of trimethylolpropanetrimethacrylate is similar to that exhibited by one of our previous resins cross-linked with 4.1% mol methylenebisacrylamide (Table 3).<sup>[24]</sup>

**Nanometer-level morphology in water—ESR analysis:** In previous papers we have extensively shown that the rotational mobility of the spin probe 2,2,6,6-tetramethyl-4-oxo-1-piperidine (TEMPONE) is a good indicator of the molecular accessibility and nanoporosity of swollen gel-type resins that result from the employment of classical bifunctional cross-linking agents.<sup>[16–18]</sup> Good indications of molecular accessibility and nanoporosity were also gathered in the case of macroreticular resins<sup>[28]</sup> and of the unconventional macro-, meso- and microporous resin polybenzimidazole.<sup>[29]</sup> When the rotation of TEMPONE is “free”, that is, hampered only by moderate microviscosity effects and not by chemisorption phenomena, the fast spin-probe reorientation is able to average out the magnetic anisotropies<sup>[30]</sup> producing a well-resolved three-line spectrum (Figure 7). Under these

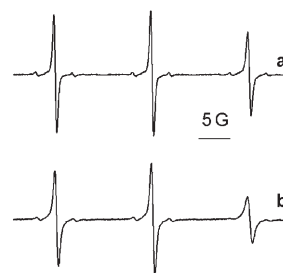


Figure 7. ESR spectra of TEMPONE in water-swollen a) MASF6 and b) AAD2 at 25°C.

conditions, the rotational correlation time  $\tau$  of the nitroxide, (obtained from the broadening of the triplet lines, see Experimental Section) provides two pieces of information. It tells us that the spin-probe does reach the nanoporous domains under exploration (i.e., they turn out to be accessible to a molecule of substantial size) and it also inversely qualitatively correlates with the average size of cavities within the investigated swollen polymer framework.<sup>[16,18]</sup> Typical motionally averaged ( $\tau = 10^{-11}$ – $10^{-9}$  s) spectra of TEMPONE inside swollen MASF6 and AAD2 are reported in Figure 7; the situation is qualitatively similar for MASF2, MASF4 and AAD1. Relevant values of  $\tau$ , hyperfine coupling constants ( $a_{\text{iso}}$ ) and activation energies ( $E_a$ ) are given in Table 4.

Table 4 shows that the decrease of average size of the nanopores located inside the swollen polymer framework, caused by the increase in the degree of cross-linking, is paralleled by a progressive decrease of spin-probe mobility (an increase of  $\tau$ ). Interestingly, the  $\tau$  values referring to AAD1 and MASF6, which have the same degree of cross-linking (Table 1), are very similar in agreement with the quite similar ISEC pattern (Tables 2 and 3). Apparently, possible additional noncovalent cross-linking, due to hydrogen bonds involving the pendant carboxylic groups of AAD1, does not appreciably modify the polymer framework accessibility. Quite in contrast with these observations, the spectrum of AAD3 collected at room temperature clearly suggests dispersion of TEMPONE in more than one environment, as

Table 4. Rotational correlation times  $\tau$ , isotropic hyperfine coupling constants  $a_{\text{iso}}$  and apparent rotational activation energies  $E_a$  of TEMPONE in water swollen resins. Data referring to AAD3 were obtained by means of spectra simulation (Figure 8a); relative intensities of the two detected spectral components are given in parenthesis.

	$\tau$ [ps] ( $\pm 5\%$ , 25°C)	$a_{\text{iso}}$ [G] ( $\pm 0.03$ )	$E_a$ [kJ mol <sup>-1</sup> ] ( $\pm 0.5$ )
bulk	11	15.88	17.8
MASF2	37	15.77	18.5
MASF4	46	15.73	18.0
MASF6	73	15.71	19.2
AAD1	67	15.69	18.2
AAD2	158	15.63	12.6
AAD3	49 (14%)	15.87	–
	419 (86%)	15.63	–

witnessed by distinct line broadening and asymmetry in the high-field line (Figure 8).

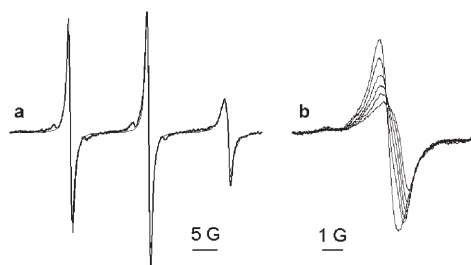


Figure 8. a) Observed (thick line) ESR spectrum of TEMPONE in water-swollen AAD3 at 25°C; simulated (thin line) ESR spectrum with parameters listed in Table 4 and 0.3 G line-width. b) Line shape changes of high-field line as temperature increases from 25°C (minimum amplitude) to 75°C (maximum amplitude) with 10°C step.

Under these conditions, to get information on the gel-phase nanomorphology, the spin-probe mobility was evaluated by means of line-shape simulation (see Experimental Section). The observed spectrum was nicely simulated by assuming a two site-model (Figure 8a). The  $\tau$  and  $a_{\text{iso}}$  values referring to the two components together with relative populations are given in Table 4. This observation implies that TEMPONE resides in two different domains in which it rotates quite “freely” (minor component) or it is subjected to relatively high microviscosity (major component). In this context, the  $\tau$  value referring to the predominant spectral contribution confirms the decreasing trend of spin-probe mobility with cross-linking given by ESR analysis of “uncomplicated” spectra (see Table 4).

The temperature dependence of the rotational diffusion is expressed in terms of the apparent activation energy  $E_a$  evaluated from Arrhenius plots. The observed  $E_a$ 's for the MASF resins and AAD1 (Table 4) approach the value of bulk water, as is typical of low cross-linked gel-type resins, for which the spin-probe reorientation mechanism is scarcely affected by the relatively low polymer chain density. A quite surprising datum is observed in the case of AAD2, which exhibits a markedly lower  $E_a$  value relative to the pure solvent. A similar behaviour was previously found in

the case of resins characterised by the coexistence of gel-type domains and larger cavities (mesopores)<sup>[28]</sup> or channels<sup>[31]</sup> and was attributed to the combined effect of molecular tumbling inside each of these two different environments and the exchange dynamics between them. The behaviour of AAD3 provides direct evidence of exchange. The fact that at 25°C individual spectral contributions are observed reveals that the exchange rate of spin-probe among the different sites is relatively slow<sup>[28,31]</sup> under these conditions. However, as temperature increases, the line shape progressively approaches the features of a single-component spectrum (Figure 8b), as expected for a fast-exchange regime.<sup>[32]</sup> Besides temperature, cross-linking can strongly affect the translational mobility of molecules dispersed inside the polymer network<sup>[18]</sup> and, consequently, the exchange rate between gel-type domains with different polymer chain density. In this context, the behaviour of AAD1 or the MASF resins seems to fall in a fast-rate limit; this is consistent with the expected relatively high permeability of the network to the spin probe molecules. Thus, under these circumstances, the line width reflects the weighted average rotational mobility of the spin-probe population, and temperature dependence provides a reliable estimation of the activation energy of the rotational diffusion. In AAD2 both rotational and exchange dynamics occur on a timescale intermediate between those of AAD1 and AAD3. We suspect that the observed seemingly single-component spectrum given by AAD2 actually consists of unresolved spectral contributions given by spin-probes located in slightly different environments and subjected to a moderately slow exchange. In this case, both reorientation and exchange dynamics produce line broadening but with opposite temperature dependence, the final result being an apparent decrease of  $E_a$ .

To further evaluate nanometer level morphology of the resins in water on the basis of ESR analysis, Cu<sup>2+</sup>(aq) was incorporated inside AAD resins as additional spin-probe. Figure 9 shows some relevant ESR spectra of AAD resins equilibrated with 0.8 wt % Cu<sup>2+</sup>(aq) corresponding to a 8:1 carboxylic group/Cu<sup>2+</sup> ratio. Incorporation of Cu<sup>2+</sup>(aq) was carried out after swelling the resin with methanol (see the Experimental Section). The ESR spectra of the AAD resins collected at room temperature after methanol removal in vacuum (Figure 9a) are very similar and reveal clear hyperfine splitting from the parallel direction, as typical of almost complete immobilised Cu<sup>2+</sup>. Line broadening and apparent “doublet” structure (see downward arrows in Figure 9a) in the parallel region suggest partitioning of Cu<sup>2+</sup> among different binding sites. At the same temperature, the ESR spectra collected after swelling with water (Figure 9b,c) still exhibits well-resolved anisotropic hyperfine structure, particularly in the case of AAD3. This is clear evidence of the fact that Cu<sup>2+</sup> undergoes an effective coordination by the carboxylate pendants that prevents the metal ion from tumbling freely and consequently leads to averaged ESR parameters. In fact, the magnetic parameters evaluated from the spectra (listed in Figure 9) are typical of Cu<sup>2+</sup> bound to oxygen ligands in a distorted octahedral configuration.<sup>[33]</sup>

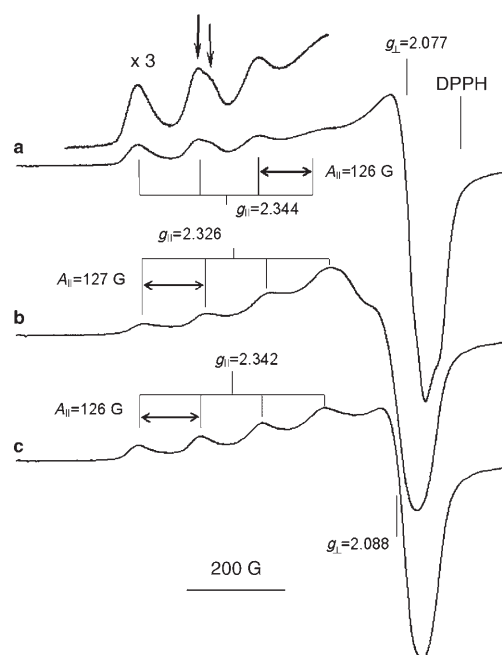


Figure 9. a) ESR spectrum at 25°C for  $\text{Cu}^{2+}$  in AAD2 in the dry state; downward arrows indicate “doublet” splitting in the parallel region. ESR spectra at 25°C for  $\text{Cu}^{2+}$  in b) AAD2 and c) AAD3 after swelling with water.

The observed  $g_{\parallel}$  and  $A_{\parallel}$  values, in view of the Peisach and Blumberg plots,<sup>[33]</sup> are compatible with a total charge of Cu complex ranging from +1 to 0, thus suggesting binding to one or two carboxylic groups, respectively. In this context, simultaneous linkage to two carboxylic groups attached to the polymer backbone is supported by the observed lower swelling of copper- and zinc-neutralised resins as compared with the swelling behaviour in water of the same resins after complete neutralisation with  $\text{Na}^{+}$ . The size of spaces hosting  $\text{Cu}^{2+}$  can significantly influence copper dynamics.<sup>[34–35]</sup> In principle, the increase of polymer-chain concentration (the decrease of cavity size) can favour multipoint linking of  $\text{Cu}^{2+}$  to the resin functionalities, on the one hand, and cause the increase of medium viscosity, on the other; the consequence of both effects is a restriction of spin-probe mobility. In water-swollen AAD3, ISEC analysis reveals essentially cavities with size comparable to that of  $\text{Cu}^{2+}(\text{aq})$ , that is, about 0.6 nm.<sup>[34]</sup> Under these conditions, both binding and physical entrapment are responsible for the almost complete immobilisation of  $\text{Cu}^{2+}$  as proved by the observed solid-type ESR spectrum. In the case of water-swollen AAD1 and AAD2 (the spectra are very similar), the solid-type spectrum overlaps onto a broad signal (Figure 9b) typical of free tumbling. This finding is consistent with the pore size distribution provided by ISEC for both AAD1 and AAD2, which, in addition to the kind of porosity observed for AAD3, reveals larger cavities (equivalent cylindrical pores with diameter of about 3 nm), inside which free reorientation of  $\text{Cu}^{2+}$  can easily occur.

**Nanomorphology in the dry and swollen state—CP/MAS  $^{13}\text{C}$  NMR spectroscopy:** The polyacrylic resins AAD1, AAD2, AAD3, MASF2, MASF4, and MASF6 were investigated by means of cross-polarization magic-angle-spinning (CP-MAS)  $^{13}\text{C}$  NMR spectroscopy to gain further insight into their nanostructure in the swollen state. Preliminarily, the CP-MAS  $^{13}\text{C}$  NMR spectra of dry resins were recorded under the conditions described in the Experimental Section. The corresponding spectroscopic data are listed in Table 5 and are compared with those of the corresponding resins swollen in water, methanol, and *n*-octanol (for MASF6 only).

Table 5. Selected CP-MAS  $^{13}\text{C}$  NMR data for MASF and AAD resins in the dry state and after swelling in different liquids ( $\text{H}_2\text{O}$ , MeOH, *n*-octanol): carbonyl and *N*-methyl chemical shift ( $\delta$ ) and the corresponding full width at half maximum ( $W_{1/2}$ ). Spectra were collected with 3 ms contact time unless otherwise stated.

	$\delta_{\text{C=O}}$ [ppm]	$W_{1/2}$ [Hz]	$\delta_{\text{N-CH}_3}$ [ppm]	$W_{1/2}$ (Hz)
MASF2				
$\text{H}_2\text{O}$	— <sup>[a]</sup>	— <sup>[a]</sup>	36.7, 34.1	— <sup>[a]</sup>
MASF4				
dry	175.3	246	37.1	313
MASF6				
dry	175.2	233	36.9	287
$\text{H}_2\text{O}$	176.9	40	38.4, 37.1	54, 41
$\text{H}_2\text{O}^{\text{[b]}}$	177.2	141	37.9, 37.3	115, 110
MeOH	176.1	53	37.3, 35.9	68, 59
MeOH <sup>[b]</sup>	176.0	49	37.3, 35.9	69, 70
<i>n</i> -octanol	175.4	105	37.6, 36.3	121, 93
<i>n</i> -octanol <sup>[b]</sup>	— <sup>[a]</sup>	— <sup>[a]</sup>	37.1	274
AAD1				
dry	175.6	258	37.1	275
$\text{H}_2\text{O}$	176.4	75	38.0, 36.7	77, 74
MeOH	174.5	80	36.3, 35.0	91, 52
AAD2				
dry	175.9	264	37.2	310
MeOH	177.0	109	38.5, 37.1	84, 68
AAD3				
dry	175.6	311	37.1	328
$\text{H}_2\text{O}$	176.1	306	37.3, 35.9	140, 119
MeOH	176.9	267	38.1, 36.7	126, 117

[a] Not recorded. [b] Contact time = 1 ms.

In the  $^{13}\text{C}$  NMR spectrum of dry MASF4 and MASF6, two main resonances are detected at  $\delta = 175.3$  and 37.1 ppm that are attributed to the nonresolved carbonyl groups of polyacrylamide and TMPTMA, and to the  $\text{N-CH}_3$  signals, respectively. Moreover spinning side bands resulting from partly averaged chemical shift anisotropy under MAS conditions are detected at the spinning rate. The signals of the methylene and methine carbon atoms of the main chain, expected at about  $\delta = 41$  and 35 ppm, likely overlap the broad  $\text{N-CH}_3$  signal. In particular, the resonance of the methylene carbons is expected to be very broad, because of the spreading of the chemical shifts of these signals due to the stereo-

irregular placement of the side groups of the polymer chain. Comparison of the MASF spectra with those of the resins of the AAD series permits the signals at  $\delta=8.5, 19.5, 24.5, 46.0$  and  $67$  ppm of the latter samples to be assigned to TMPTMA. The intensity of these resonances actually increases as the TMPTMA molar fraction in the copolymer increases, thus suggesting their attribution to the cross-linking agent. A tentative assignment of these carbon atoms is given in Table 6.

Table 6. CP-MAS  $^{13}\text{C}$  NMR chemical shift ( $\delta$ ) observed in AAD resins and attributed to the cross-linking agent TMPTMA.

$\delta$ [ppm]		$\delta$ [ppm]	
8.5	$\text{H}_3\text{C}-\text{CH}_2-\text{C}-$	24.5	$\text{H}_3\text{C}-\text{C}-\text{CH}_2-\text{C}-$
19.5	$\begin{array}{c} \text{O} \\ \parallel \\ -\text{C}-\text{C}-\text{C}- \\   \quad   \\ \text{CH}_3 \end{array}$	46.0	$-\text{C}-$
		67.0	$-\text{C}-\text{CH}_2-\text{O}-\text{C}-\text{O}$

The AAD resins were synthesised by employing MA comonomer. The MA concentration in the polymer can be only indirectly deduced by integration of the  $^{13}\text{C}$  NMR signals, since MA resonances are not resolved from those of TMPTMA. In fact the intensity ratio of peaks at about  $\delta=9$  ppm ( $-\text{CH}_3$ ) and  $65$  ppm ( $-\text{CH}_2-\text{O}-$ ) match the TMPTMA composition very well, whereas other signals at about  $\delta=20$  and  $45$  ppm are more intense, due to overlapping with the MA resonances. This method is evidently not a rigorous one and it permits only a rough evaluation of the monomer composition, assuming the same proportionality of all  $^{13}\text{C}$  NMR spectral lines with their molar concentration in the polymer. However, the observed values are in good agreement with data resulting from elemental analysis, probably as a result of the short contact time of  $1$  ms employed in recording the CP-MAS  $^{13}\text{C}$  NMR spectra.

The resins are thus swollen in solvents with different solvating properties, namely water, methanol, and *n*-octanol, under conditions described in the Experimental Section. MASF6 is investigated in greater detail as representative example of the resins. The CP-MAS  $^{13}\text{C}$  NMR spectra of the dry resin and of the resin swollen in methanol swollen are compared in Figure 10.

A solvent effect on the line width ( $W_{1/2}$ ) of the  $^{13}\text{C}$  signals is clearly observed: both carbonyl and  $\text{N}-\text{CH}_3$  resonances are narrower in the gel than in solid state, and the signal line width decreases as the solvating properties of the solvent increases as a result of the decrease of  $^1\text{H}/^1\text{H}$  dipolar interaction and increased mobility of the polymer chain.<sup>[36]</sup> Actually the  $W_{1/2}$  values of the carbonyl groups range from  $233$  Hz in the solid state to  $40$  and  $53$  Hz, in water and methanol gels, respectively. A comparable trend is observed for the  $\text{N}-\text{CH}_3$  signals in the same solvents. In higher alkyl alcohol solvents, for example, *n*-octanol, the solvating effects are

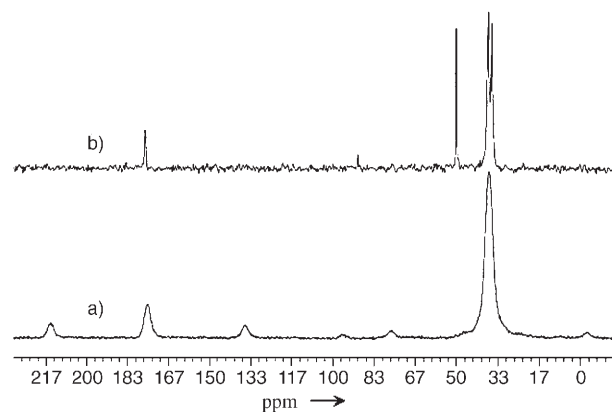


Figure 10. CP-MAS  $^{13}\text{C}$  NMR spectra of the resin MASF6 a) dry and b) swollen in methanol. Both spectra were recorded by using  $3$  ms contact time (CT) and  $5$  s repetition time.

small and the line width of the quoted signals increased to about the half value of the solid state.

As discussed in the previous sections, the gel swollen in water can yield a relatively dense volume as a result of the reduced accessibility of some nanoporous domains to the solvent molecules. Actually the line width of the  $^{13}\text{C}$  signals is found to be dependent on solvent and contact time used in the cross polarization pulse sequence. In methanol gel the  $W_{1/2}$  values remain unchanged ( $40$ – $55$  Hz) at contact times of  $1$  and  $3$  ms, whereas they increase in water gel approaching a value half of that of the solid state value ( $140$  vs  $240$  Hz) when the shorter contact time of  $1$  ms is used. A broad line width is still observed for the sample swollen in *n*-octanol at a contact time of  $3$  ms. Methanol exhibits evident good solvating properties, thus enabling elevated and homogeneous mobility of the polymer backbone as well as of the side groups: this is confirmed by the lack of the spinning side bands for carbonyl and  $\text{N}-\text{CH}_3$  signals and by an increased spectral resolution at any contact time that permits two signals for the nonequivalent  $\text{N}-\text{CH}_3$  carbons to be detected. Moreover the  $^{13}\text{C}$  NMR signal of methanol is at  $\delta=50.3$  ppm and its intensity increases as contact time is increased from  $1$  to  $3$  ms. This increase is the result of the reduced mobility of solvent molecules located nearby the macromolecular chain: indeed a longer contact time for the growth of this signal during the cross polarization time is needed. Gels of MASF6 in water and *n*-octanol are seen to be heterogeneous in nature and domains with different mobility of the polymer chain are detected. As a matter of fact complex cross polarization dynamics are observed which produce a line width of the signals that is dependent on the contact time.<sup>[36]</sup> It is worth noting that in the CP/MAS  $^{13}\text{C}$  NMR spectrum of MASF6 gel in water, recorded with a contact time of  $3$  ms, two signals at  $\delta=38.5$  and  $36$  ppm are detected and attributed to the main chain methylene and methine carbon atoms: these signals are not found in the spectra of the methanol gel, even when the contact time is varied. The reduced polymer chain mobility in water permits an efficient cross polarization of the signals due to



these carbon atoms that are thus now observable. In methanol gel the high mobility of the swollen polymer chain produces a fast relaxation of the  $^{13}\text{C}$  nuclei and fast decay of the signal intensity during the contact time yielding a non-efficient cross polarization process.

Three samples characterised by increasing molar concentration of the cross-linking agent TMPTMA, namely AAD1–3, were also analyzed. The increased degree of cross-linking reduces, as expected, the chain mobility and the access of the solvent molecules to the polymer chain. Hence, an increase of the line width of the carbonyl and of the N-CH<sub>3</sub> signals is expected and actually detected as the TMPTMA content in the polymer sample increases (see Table 5). The line width of the carbonyl  $^{13}\text{C}$  NMR signals of the resin AAD3, containing the highest molar fraction of TMPTMA, is about the same for dry and swollen resin. In contrast, when the concentration of the cross-linking agent is reduced, a significant reduction of the line width is observed and the  $W_{1/2}$  values approach those found in the spectra of the MASF series.

## Conclusion

Functional gel-type acrylic resins with polymethylene chains featured by *N,N*-dimethylamido and carboxylic pendants, and interconnected with a trifunctional cross-linker (0.6 to 7.0% mol), exhibit (with the partial exception of AAD3) an essentially uncomplicated homogeneous polymer framework, after being swollen with water and examined with ISEC and ESR techniques. These techniques provide a convergent picture of a homogeneous macromolecular three-dimensional structure that is featured by “nanopores” potentially able to play a decisive role in controlling the growth of metal nanoclusters<sup>[22]</sup> ranging from 2 to 4 nm in diameter. In its turn, the preliminary analysis of the polymer gels by CP-MAS  $^{13}\text{C}$  NMR spectroscopy permitted us to describe qualitatively the solvating properties of the polymer chain at variance of solvents exhibiting different polarity. Complementary information consistent with those given by ISEC and ESR are actually provided by this technique. Thus, 1) the accessibility of the nanoporous domains to molecules of substantial size is confirmed in water and in methanol by ISEC and ESR analysis; water and methanol are seen by CP-MAS  $^{13}\text{C}$  NMR spectroscopy to produce a sort of pseudo-solution state; 2) the structural homogeneity perceived by ESR spectroscopy is confirmed by CP-MAS  $^{13}\text{C}$  NMR spectroscopy of the sample in methanol but not in water, in which clear evidence of an appreciable inhomogeneity are observed; and 3) the increase in the degree of cross-linking is accompanied by a decrease of the solvation of the polymer chains revealed by CP-MAS  $^{13}\text{C}$  NMR spectroscopy, in line with the observed decrease of porosity clearly evidenced by ISEC analysis.

## Experimental Section

**TGA experiments:** TG-IR analyses were carried out with an SDT2960 thermobalance (TA Instruments) coupled with a Nicolet Nexus FT-IR apparatus, equipped with a Nicolet TGA interface. TG curves were recorded under a working N<sub>2</sub> flux equal to 70 cm<sup>3</sup> min<sup>-1</sup>, with a heating rate equal to 20 °C min<sup>-1</sup>. The measurements were carried out on about 10 mg of sample in an open alumina pan.

**ISEC analysis:** D<sub>2</sub>O, sugars, and polydextrans were employed as standard solutes in ISEC characterisation of water-swollen resins. Details of the experimental procedure and data treatment were reported elsewhere.<sup>[16–18]</sup>

**ESR measurements:** About 50 mg of ground material were swollen with a 1.5 · 10<sup>-4</sup> M aqueous solution of the paramagnetic probe TEMPONE (90–95% from Sigma) under nitrogen. The sample was allowed to reach the swelling equilibrium, and after pouring the suspension onto filter paper to remove the excess solution, a suitable amount of swollen material was quickly transferred into the ESR tube. The ESR spectra were recorded using an X-band JEOL JES-RE1X apparatus working at 9.2 GHz (modulation 100 kHz) over the temperature range 5–50 °C at 5 °C steps. The temperature of the sample was controlled by a variable-temperature unit Steler VTC91, the accuracy being ±0.1 °C. The spectra of the spin-probe generally appear as those typical of a fast-motion regime.<sup>[30]</sup> Under these conditions, the rotational correlation time  $\tau$  of TEMPONE was calculated according to the formula given in Equation (1),<sup>[30,37]</sup> in which  $\omega_c = 5.78 \cdot 10^{10}$  Hz; the parameters  $h_{+1}$ ,  $h_0$  and  $h_{-1}$  (the intensities of the low-, middle-, and high-field lines, respectively) and  $\Delta H_0$  (the peak-to-peak width of the central line) were obtained by peak-picking from the first derivative spectrum.

$$\tau = 6.14 \cdot 10^{-10} \Delta H_0 [(h_0/h_{+1})^{1/2} + (h_0/h_{-1})^{1/2} - 2][1 - 0.2(1 + \omega_c^2 \tau^2)] \quad (1)$$

The numerical constant of Equation (1) (in units of s G<sup>-1</sup>) was evaluated on the basis of the components of the hyperfine **A** tensor observed in single crystals:<sup>[38]</sup>  $A_x = 5.5$  G,  $A_y = 5.8$  G,  $A_z = 32.5$  G. To account for polarity effects, the right hand side of Equation (1) was multiplied by  $(a_N/a_{\text{iso}})^2$  in which  $a_N = (A_x + A_y + A_z)/3$  and  $a_{\text{iso}}$  is the hyperfine isotropic term evaluated from the observed splitting in motionally averaged spectra. The computer program NLSL<sup>[39]</sup> was used to simulate bimodal spectra assuming Brownian isotropic reorientation of the spin-probe and Lorentzian line-shape. The magnetic parameters observed in single crystal<sup>[38]</sup> were used in line-shape simulation, but the **A** tensor components were properly scaled to fit the observed splitting. A well established protocol<sup>[40]</sup> based on the reaction with copper acetate and concomitant release of acetic acid was used to prepare magnetically diluted samples of Cu<sup>2+</sup> in AAD resins. One gram resin was pre-swollen in 10 mL of methanol, then suitable aliquot amounts of a solution of Cu(OOCCH<sub>3</sub>)<sub>2</sub> and Zn(OOCCH<sub>3</sub>)<sub>2</sub> in methanol were added to give the complete neutralisation of carboxylic groups of the resin with Cu<sup>2+</sup> and Zn<sup>2+</sup> and a desired Cu<sup>2+</sup> content. The mixture was gently stirred at room temperature for 30 min, after which time the resin was separated by filtration, washed with methanol and dried at 50 °C under vacuum to constant weight. The X-band ESR spectra of Cu<sup>2+</sup> were recorded at 25 °C in the spectral range 2400–3400 G. Calibration of *g* values was based on DPPH (DPPH =  $\alpha, \alpha'$ -diphenyl- $\beta$ -picrylhydrazyl) ( $g = 2.0036$ ).

**Solid-state CP-MAS  $^{13}\text{C}$  NMR spectroscopy:** Solid-state CP-MAS  $^{13}\text{C}$  NMR spectra were recorded at room temperature on a Bruker AMX300 spectrometer (75.46 MHz for  $^{13}\text{C}$ ) by using high power decoupling and standard cross-polarization techniques. The magic angle was calibrated with KBr side bands and the samples were spun at 5 kHz in 4 mm diameter zirconia rotors equipped with Kel-F caps. Approximately 2000 scans were collected by using 90° pulse (3.4  $\mu$ s), 1, 3 or 5 ms cross-polarization contact time (for the specific value used see the text and Table 5), 5 s recycle delay, and 2k data points with zero filling to 16 K corresponding to an acquisition time of 45 ms. The free induction decays were processed with a 10 Hz exponential line broadening. The  $^{13}\text{C}$  chemical shifts are referenced to tetramethylsilane at  $\delta = 0$  ppm using the

methyl signal of sodium 3-(trimethyl-silyl)-1-propane sulfonate as external reference.

**Materials:** All reagents and solvents were of reagent grade and were used as received.

**Resin synthesis:** Resins were prepared upon  $\gamma$ -ray irradiation of designed mixtures of the comonomers DMMA and MA (both from Aldrich, 99%) and the cross-linker TMPTMA (Polysciences, 99%). The monomers mixtures were prepared in screw-capped glass vials and, after air removal with dinitrogen, they were exposed to  $\gamma$ -rays from a  $^{60}\text{Co}$  source at 0.12 Gy s<sup>-1</sup> at room temperature and at a distance of 22 cm for 24 h. The resulting clear rods were thoroughly crushed in a glass mortar under methanol, extensively washed with the same solvent, vacuum dried and, after further dry grinding with an impact grinder, sieved to a particle size of 400–180  $\mu\text{m}$ . Elemental analyses (C, H, N) of the samples were carried out by means of a Carlo Erba 1106 analyzer. Details are provided in Table 7.

Table 7. Synthetic data (elemental analysis) for the resins MASF and AAD.

	C [%] <sup>[a]</sup>	H [%] <sup>[a]</sup>	N [%] <sup>[a]</sup>	Yield [%]
MASF2	59.59 (60.64)	9.07 (9.12)	13.62 (13.85)	94
MASF4	59.24 (60.70)	9.09 (9.09)	13.43 (13.58)	97
MASF6	59.50 (60.75)	9.21 (9.06)	13.01 (13.32)	96
AAD1	59.53 (60.55)	8.43 (8.97)	12.34 (12.71)	96
AAD2	59.44 (60.73)	8.62 (8.89)	11.56 (11.94)	94
AAD3	59.61 (61.05)	8.70 (8.76)	10.23 (10.59)	97

[a] Calculated theoretical values are given in parentheses and are based on 100% polymerisation yield.

### Acknowledgements

The contribution of Dr. Patrizia Oliva for recording the CP-MAS NMR spectra of our resins is gratefully acknowledged. Financial support from the project AS CR No. K4050111 to K.J. is gratefully acknowledged.

[1] See for example M. Haruta, *Gold Bull.* **2004**, *37*, 27–36.  
 [2] *Synthesis and Separations using Functional Polymers* (Eds.: D. C. Sherrington, P. Hodge), Wiley, New York, **1988**.  
 [3] *Ion-exchangers* (Ed.: K. Dorfner), de Gruyter, Berlin, **1991**.  
 [4] B. Corain, M. Zecca, K. Jeřábek, *J. Mol. Catal. A* **2001**, *177*, 3–20.  
 [5] B. Corain, M. Kralik, *J. Mol. Catal. A* **2000**, *159*, 153–162.  
 [6] P. Hodge, *Chem. Soc. Rev.* **1997**, *26*, 417–424.  
 [7] M. Ohtaki, M. Komiyama, H. Hirai, N. Toshima, *Macromolecules* **1991**, *24*, 5567–5572.  
 [8] B. Corain, P. Centomo, S. Lora, M. Kralik, *J. Mol. Catal. A* **2003**, *204/205*, 755–762, and references therein.  
 [9] C. Burato, P. Centomo, G. Pace, M. Favaro, L. Prati, B. Corain, *J. Mol. Catal. A* **2005**, *238*, 26–34.  
 [10] P. Centomo, S. Lora, M. Zecca, G. Vitulli, A. M. Caporusso, S. Galvagno, C. Milone, B. Corain, *J. Catal.* **2005**, *229*, 283–297.  
 [11] F. Shi, Y. Deng, *J. Catal.* **2002**, *211*, 548–551.  
 [12] Y. Uozumi, R. Nakao, *Angew. Chem.* **2003**, *115*, 204–207; *Angew. Chem. Int. Ed.* **2003**, *42*, 194–197.

[13] G. Brieve, E. C. Serrano, J. M. Campos-Martin, L. G. Fierro, *Chem. Commun.* **2004**, 1184–1185.  
 [14] C. Burato, P. Centomo, M. Rizzoli, A. Biffis, S. Campestrini, B. Corain, unpublished results.  
 [15] a) K. Jeřábek, *Anal. Chem.* **1985**, *57*, 1595–1597; b) K. Jeřábek, *Anal. Chem.* **1985**, *57*, 1598–1602; c) K. Jeřábek, K. Setinek, *J. Polym. Sci. Part A* **1990**, *28*, 1387; d) K. Jeřábek, *ACS Symp. Ser.* **1996**, *635*, 211–224.  
 [16] A. Biffis, B. Corain, M. Zecca, C. Corvaja, K. Jeřábek, *J. Am. Chem. Soc.* **1995**, *117*, 1603–1606.  
 [17] M. Zecca, A. Biffis, G. Palma, C. Corvaja, S. Lora, K. Jeřábek, B. Corain, *Macromolecules* **1996**, *29*, 4655–4661.  
 [18] A. A. D'Archivio, L. Galantini, A. Panatta, E. Tettamanti, B. Corain, *J. Phys. Chem. B* **1998**, *102*, 6774–6779.  
 [19] S. Pickup, F. D. Blum, W. T. Ford, M. Peryiasamy, *J. Am. Chem. Soc.* **1986**, *108*, 3987–3990.  
 [20] A. G. Ogston, *Trans. Faraday Soc.* **1958**, *54*, 1754–1757.  
 [21] M. Kralik, V. Kratyk, M. De Rosso, M. Tonelli, S. Lora, B. Corain, *Chem. Eur. J.* **2003**, *9*, 209–214.  
 [22] B. Corain, K. Jeřábek, P. Centomo, P. Canton, *Angew. Chem.* **2004**, *116*, 977–980; *Angew. Chem. Int. Ed.* **2004**, *43*, 959–962.  
 [23] B. Corain, C. Burato, P. Centomo, S. Lora, W. Meyer-Zaika, G. Schmid, *J. Mol. Catal. A* **2005**, *225*, 189–195.  
 [24] F. Artuso, A. A. D'Archivio, S. Lora, K. Jeřábek, M. Kralik, B. Corain, *Chem. Eur. J.* **2003**, *9*, 5292–5296.  
 [25] M. Valenius, L.-I. Kulin, P. Flodin, *React. Polym.* **1992**, *17*, 309–323.  
 [26] M. Glad, P. Reinholdsson, K. Mosbach, *React. Polym.* **1995**, *25*, 47–54.  
 [27] P. M. van Berkel, S. C. van der Slot, W. L. Driessen, J. Reedijk, D. C. Sherrington, *Eur. Polym. J.* **1997**, *33*, 303–310.  
 [28] A. A. D'Archivio, L. Galantini, E. Tettamanti, A. Panatta, B. Corain, *J. Mol. Catal. A* **2000**, *157*, 269–273.  
 [29] A. A. D'Archivio, L. Galantini, A. Biffis, K. Jeřábek, B. Corain, *Chem. Eur. J.* **2000**, *6*, 794–799.  
 [30] P. L. Nordio in *Spin Labeling, Theory and Applications, Vol. I* (Ed.: L. J. Berliner), Academic Press, New York, **1976**, pp. 5–52.  
 [31] A. A. D'Archivio, L. Tauro, L. Galantini, A. Panatta, E. Tettamanti, M. Giammatteo, K. Jeřábek, B. Corain, unpublished results.  
 [32] J. A. Weil, J. R. Bolton, J. E. Wertz, *Electron Paramagnetic Resonance*, Wiley Interscience, **1994** pp. 304–309.  
 [33] J. Peisach, W. E. Blumberg, *Arch. Biochem. Biophys.* **1974**, *165*, 691–708.  
 [34] D. Suryanarayana, P. A. Narayana, L. Kevan, *Inorg. Chem.* **1983**, *22*, 474–478.  
 [35] G. C. Rex, S. Schlick, *J. Phys. Chem.* **1985**, *89*, 3598–3601.  
 [36] a) S. Lai, E. Locci, G. Saba, I. Husu, G. Masci, V. Crescenzi, A. Lai, *J. Polym. Sci. Part A* **2003**, *41*, 3123–3131; b) R. M. Hodge, T. J. Bastow, G. H. Edward, G. P. Simon, A. J. Hill, *Macromolecules* **1996**, *29*, 8137–8143; c) G. Metz, M. Ziliox, S. O. Smith, *Solid State Nucl. Magn. Reson.* **1996**, *7*, 155–160.  
 [37] a) B. D. Chestnut, J. F. Hower, *J. Phys. Chem.* **1971**, *75*, 907–912; b) M. F. Ottaviani, *J. Phys. Chem.* **1987**, *91*, 779–784.  
 [38] M. Brustolon, A. L. Maniero, C. Corvaja, *Mol. Phys.* **1984**, *51*, 1269–1281.  
 [39] D. E. Budil, S. Lee, S. Saxena, J. H. Freed, *J. Magn. Reson. Ser. A* **1996**, *120*, 155–189.  
 [40] a) D. Belli Dell'Amico, S. Lora, A. A. D'Archivio, L. Galantini, A. Biffis, B. Corain, *J. Mol. Catal. A* **2000**, *157*, 173–181; b) F. Filippi, G. Palma, S. Lora, C. Maccà, B. Corain, *J. Mol. Catal. A* **2003**, *203*, 213–220.

Received: June 13, 2005  
Published online: August 31, 2005